a-axis optical conductivity of detwinned ortho-II $YBa_2Cu_3O_{6.50}$

J. Hwang,[1] J. Yang,[1] T. Timusk,[1,*] S. G. Sharapov,[1] J. P. Carbotte,[1] D. A. Bonn,[2] Ruixing Liang,[2] and W. N. Hardy[2]
[1]*Department of Physics and Astronomy, McMaster University, Hamilton, Ontario L8S 4M1, Canada*
[2]*Department of Physics and Astronomy, University of British Columbia, Vancouver, British Columbia V6T 1Z1, Canada*
(Received 10 May 2005; revised manuscript received 8 November 2005; published 10 January 2006)

The *a*-axis optical properties of a detwinned single crystal of $YBa_2Cu_3O_{6.50}$ in the ortho-II phase (Ortho-II Y123, $T_c=59$ K) were determined from reflectance data over a wide frequency range (70–42 000 cm^{-1}) for nine temperature values between 28 and 295 K. Above 200 K the spectra are dominated by a broad background of scattering that extends to 1 eV. Below 200 K a shoulder in the reflectance appears and signals the onset of scattering at 400 cm^{-1}. In this temperature range we also observe a peak in the optical conductivity at 177 cm^{-1}. Below 59 K, the superconducting transition temperature, the spectra change dramatically with the appearance of the superconducting condensate. Its spectral weight is consistent, to within experimental error, with the Ferrell-Glover-Tinkham (FGT) sum rule. We also compare our data with magnetic neutron scattering on samples from the same source that show a strong resonance at 31 meV. We find that the scattering rates can be modeled as the combined effect of the neutron resonance and a bosonic background in the presence of a density of states with a pseudogap. The model shows that the decreasing amplitude of the neutron resonance with temperature is compensated for by an increasing of the bosonic background yielding a net temperature-independent scattering rate at high frequencies. This is in agreement with the experiments.

DOI: 10.1103/PhysRevB.73.014508 PACS number(s): 74.25.Gz, 74.25.Kc, 74.72.Bk

The complete phase diagram of the high temperature superconducting (HTSC) cuprates is still under intense debate. The normal state, particularly in the underdoped region, is dominated by a variety of not-well-understood crossover phenomena that may either be precursors to superconductivity or competing states. These include the pseudogap,[1] the magnetic resonance,[2–4] the anomalous Nernst effect,[5,6] stripe order,[7–10] and possible superconducting fluctuations.[11,12] The situation is further complicated by the presence of disorder and the practical considerations that lead to a situation where a given cuprate is not investigated with all the available experimental techniques. Ideally, one would like to have a system where disorder is minimized and several experimental techniques can be used with the same crystals. As a step in that direction we present detailed *a*-axis optical data on the highly ordered ortho-II phase of $YBa_2Cu_3O_{6.50}$ (Ortho-II Y123) and compare these data with recent results from magnetic neutron scattering, microwave spectroscopy, and dc resistivity on crystals from the same source.

An important motivation for a comparison between transport properties and the magnetic neutron resonance comes from the suggestion that the carrier lifetime, as measured by infrared spectroscopy, is dominated by a bosonic mode[13–17] whose frequency and intensity, as a function of temperature and doping level, tracks the inelastic magnetic resonance at 41 meV with in-plane momentum transfer of (π,π).[15,16] The magnetic resonance has also been invoked to explain other self-energy effects such as the kink in the dispersion of angle-resolved photoemission spectra[18–21] (ARPES) and as a hump-peak structure in tunneling spectra.[22] These effects have also been attributed to the electron-phonon interaction.[23] While the bosonic excitation may not be the fundamental engine of superconductivity,[16,24] it is, nevertheless, important to map out the regions in the phase diagram where it can be found and correlate the various experiments that yield evidence of its presence.

The $YBa_2Cu_3O_{7-x}$ (Y123) material has been one of the most thoroughly studied of all the HTSC systems but, like most cuprates, it suffers from disorder associated with the charge reservoir layer, in the case of Y123, disordered oxygen chains. However, at an oxygen doping level of $x=0.50$, an ordered ortho-II phase occurs with alternating full and empty CuO chains, doubling the unit cell along the *a* direction, and yielding a well ordered stoichiometric compound.[25,26] A further advantage of this system is the availability of very large crystals, suitable for neutron scattering. A disadvantage of the Y123 system is that the crystals are not easily vacuum cleaved and as a result, surface sensitive probes, such as angle resolved photoemission or scanning tunneling microscopy, have been used less with Y123. In contrast, $Bi_2Sr_2CaCu_2O_8$ (Bi-2212) cleaves easily and unlike Y123, can also be overdoped. Optical spectroscopy has the advantage of working on both systems equally well and offers a bridge between the ARPES surface sensitive experiments and the large-volume probe of neutron scattering.

The paper is organized as follows. We start with a brief introduction to the experimental method followed by a presentation of the raw reflectance data and an analysis where we use the extended Drude model to extract the various optical constants, in particular the real and imaginary parts of the scattering rate. We first remove known features in the conductivity spectra, the transverse optical phonons. The measured scattering rates are then compared with a theoretical model. We next discuss the overall results by comparing them with data from other experiments on Ortho-II Y123, in particular recent neutron data[27] on samples from the same source.

I. EXPERIMENTAL METHOD AND RESULTS

The detwinned ortho-II $YBa_2Cu_3O_{6.50}$ sample used in this study was grown by a flux method using $BaZrO_3$ crucibles,[28]

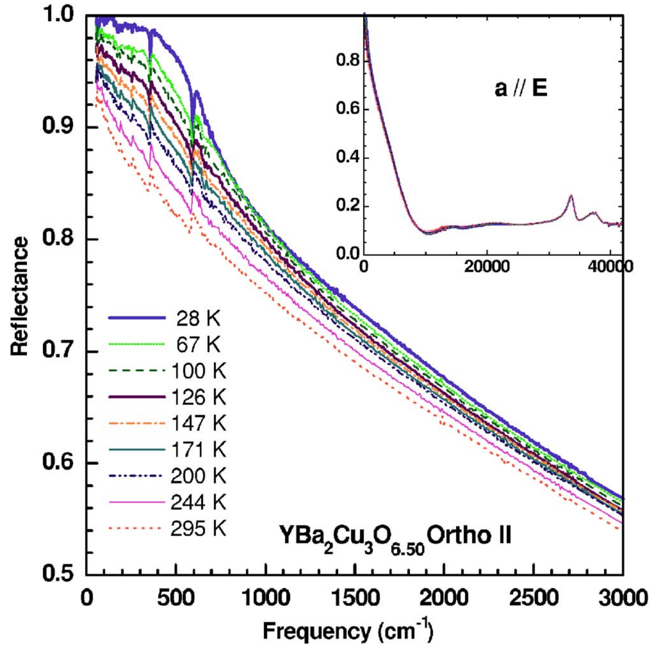

FIG. 1. (Color online) The a-axis reflectance of Ortho-II Y123 at nine temperatures. There is a broadband of absorption giving rise to a region of negative curvature of the reflectance between 350 and 600 cm^{-1}. At high temperature the curvature is positive at all frequencies. The inset shows the high frequency reflectance.

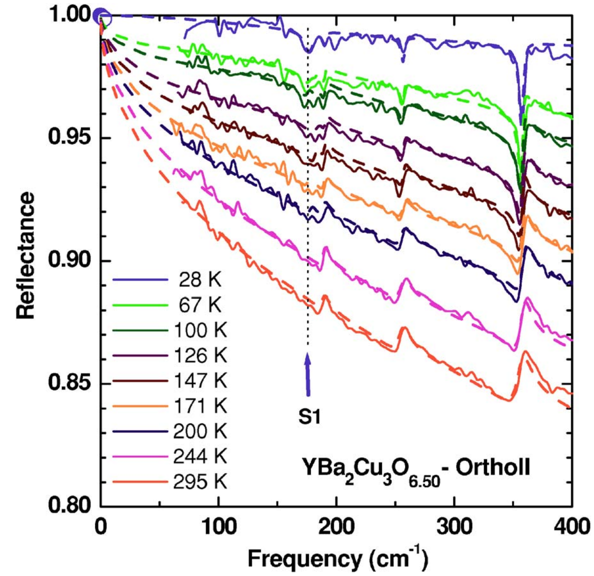

FIG. 2. (Color online) The measured low frequency reflectance is shown as solid lines and an oscillator fit is shown as dashed lines. The data are fitted with two Drude bands and a series of oscillators, one of which is a strong electronic mode marked $S1$. In the superconducting state an oscillator at zero frequency represents the superconducting condensate. The oscillator parameters are shown in Table I. The open circles near zero frequency are reflectance data at 28 K from a microwave measurement (Ref. 33).

annealed under pure oxygen gas flow at 760 °C, and detwinned at 300 °C by applying uniaxial stress of 100 atm along the a direction.[25] The dimension of the sample is 1.5 $\times 1 \times 0.2$ mm^3. The nearly normal-incident reflectance of the sample was measured over a wide frequency range (70–42 000 cm^{-1}) at nine temperatures between 28 K and 295 K with a Bruker IFS 66v/S Fourier transform spectrometer with linearly polarized light. The technical reason for the 28 K lower temperature limit is a nylon screw that rigidly clamps our sample holder, giving excellent mechanical stability, but also increases the heat flow to the ambient and limits to lowest attainable temperatures. A polished stainless steel mirror was used as an intermediate reference to correct for instrumental drifts with time and temperature. An *in situ* evaporated gold film on the sample was the absolute reflectance reference.[29] The reflectance of the gold films was in turn calibrated with a polished stainless steel sample where we relied on the Drude theory and the dc resistivity as the ultimate reference. An advantage of this technique is that it corrects for geometrical effects of an irregular surface. The *in situ* gold evaporation technique gives an absolute accuracy of the reflectance of better than ±0.5%. For the reflectance data above 14 000 cm^{-1} we used aluminum instead of gold as the coating material.

Figure 1 shows the raw reflectance data for nine different temperatures in the frequency region from 75 cm^{-1} to 3000 cm^{-1}. The inset extends the data up to 42 000 cm^{-1}. A strong temperature dependence is observed in the low frequency range but becomes weaker at higher frequencies. Two specific features show temperature-dependent amplitudes: a broad shoulder at $\approx$400 cm^{-1} and a less obvious depression in reflectance at 175 cm^{-1}. In addition, signatures of well-known transverse optical phonons can be seen as sharp minima in the low temperature spectra.[30–32] At low temperature the overall curvature of the reflectance is negative at low frequencies changing to a positive curvature at high frequency, which gives rise to an inflection point at $\approx$700 cm^{-1}. The inset shows the high frequency reflectance with a prominent plasma edge at 13 000 cm^{-1} and a relatively weak temperature dependence above 25 000 cm^{-1}.

Figure 2 shows the lowest frequency range on an expanded scale. In addition to the transverse phonons, we observe a feature at 175 cm^{-1}, which appears below 171 K and is denoted $S1$. The thin lines are the measured reflectance curves and the dashed lines are oscillator fits where the phonons have been modeled as Drude-Lorentz oscillators. The electronic background is represented as the sum of two Drude peaks in the normal state and a two-fluid model with the narrower Drude peak replaced by a δ function at the origin in the superconducting state. The parameters used in the fit are shown in Table I. From the fit we get a superconducting condensate density of 72×10^6 cm^{-2} expressed as the square of a plasma frequency in cm^{-1}. This corresponds to a penetration depth of 1900 Å. In comparison, the recent Gd zero-field electron spin resonance (ESR) measurements on samples from the same source yield a penetration depth of 2000 Å and are shown as open circles at a very low frequency at 28 K.[33] Our estimated overall error in the absolute value of the reflectance of ±0.5% translates to a ±300 Å error in penetration depth. We conclude that our data are in agreement with the ESR results, consistent with errors associated with the measurement of absolute reflectance. From this comparison with the ESR we can conclude that our con-

TABLE I. The fitting parameters of Ortho-II Y123 reflectance at three temperatures, $T=28$ K, 100 K, and 295 K. The unit of ω_{pj}, ω_j, and γ_j is cm^{-1}. Two Drude bands Drude1 and Drude2 are used. The Drude1 band forms the superconducting condensate below T_c. The peak $S1$ splits at 100 K into two components.

	28 K			100 K			295 K		
	ω_{pj}	ω_j	γ_j	ω_{pj}	ω_j	γ_j	ω_{pj}	ω_j	γ_j
Drude1	8500	0	0	6900	0	73			
Drude2	5400	0	310	10500	0	1500	17500	0	3300
Phonons	430	190	3	500	190	4	225	189	7
	470	257	3.5	400	257	3	350	255	10
	720	358	4	690	358	3.5	520	356	13
	549	599	13	555	598	15	430	587	17
$S1$	950	178	9	470	175	6			
				355	182	4.5			
$\epsilon_\infty=3.63$									

ductivity is high by 10%. On the other hand, from a comparison with the dc conductivity (see Fig. 10) our conductivity is about 7% too low. We conclude that our overall uncertainty in the absolute value of the conductivity is about ±10%.

If we assume an overall monotonic variation of the fitted curves with temperature, we can estimate, from the deviation from this monotonicity, a relative error of 0.2% for the temperature dependence of the reflectance. Finally, from the noise level of the spectra, estimated to be 0.05% at 300 cm^{-1} and rising to 0.3% at 100 cm^{-1}, we can try to estimate an upper limit on the strength of any phonon lines that we may have missed. We note, from Table I, that typical phonons in our material have a plasma frequency of the order of 400 cm^{-1} or higher. Based on our noise level we can set an upper limit of 250 cm^{-1} to the plasma frequency of any unobserved phonon features in the spectral region $\omega > 200$ cm^{-1}. In other words, there could be more phonons than what is shown in Table I provided their plasma frequencies are less than 250 cm^{-1}. This limit would be higher at lower frequencies.

The optical conductivity and the other optical constants were determined from the measured a-axis reflectance by Kramers-Kronig analysis,[34] for which extrapolations to $\omega \to 0$ and ∞ must be supplied. For $\omega \to 0$, the reflectance was extrapolated by assuming a Hagen-Rubens frequency dependence in the normal state, $(1-R) \propto \omega^{1/2}$, and below T_c an $(1-R) \propto \omega^4$ extrapolation was used. We used the oscillator fits shown in Fig. 2 to investigate the sources of error arising from the low frequency extrapolations. The reflectance was extended to high-frequency (between 40 000 and 350 000 cm^{-1}) using data from Romberg *et al.*[35] Free-electron behavior ($R \propto \omega^{-4}$) was assumed to hold at higher frequencies.

The top panel of Fig. 3 displays the optical conductivity for the nine temperatures, eight in the normal state and one in the superconducting state. The optical conductivity can be written as $\sigma(\omega) = -i\omega[\epsilon(\omega) - \epsilon_H]/4\pi$ where ϵ_H is the dielectric constant at a high frequency (~2 eV). At all temperatures we observe four sharp phonon modes out of the six infrared active phonon modes[30–32] expected for this polarization of the incident radiation. The phonons have been labeled $P1-P4$ in the figure. We fitted the optical conductivity of these lines with a Drude-Lorentz model and found the line intensities to be temperature independent and of a magnitude expected for transverse optic (TO) phonons. Table I shows the parameters of the model.

The bottom panel of Fig. 3 shows the optical conductivity without the four phonon modes obtained through the subtraction of the fitted Drude-Lorentz conductivities from the measured conductivity. Several features stand out. First, there is a prominent onset of conductivity that appears at low temperature around 400 cm^{-1}. This feature is common to all cuprate superconductors and was assigned early on as an onset of scattering from a bosonic mode.[13,14,36] Second, a strong peak at ≈ 180 cm^{-1}, designated $S1$, grows as the temperature is

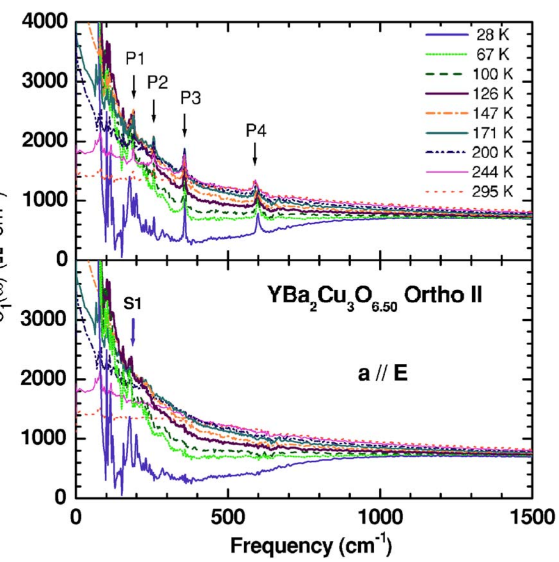

FIG. 3. (Color online) The upper panel shows the optical conductivity where several prominent phonon peaks have been identified as $P1$, $P2$, etc. In the lower panel the phonon peaks ($P1$ to $P4$) have been removed. A complex set of absorption bands can be seen at low temperature dominated by a broad peak at 177 cm^{-1} designated as $S1$.

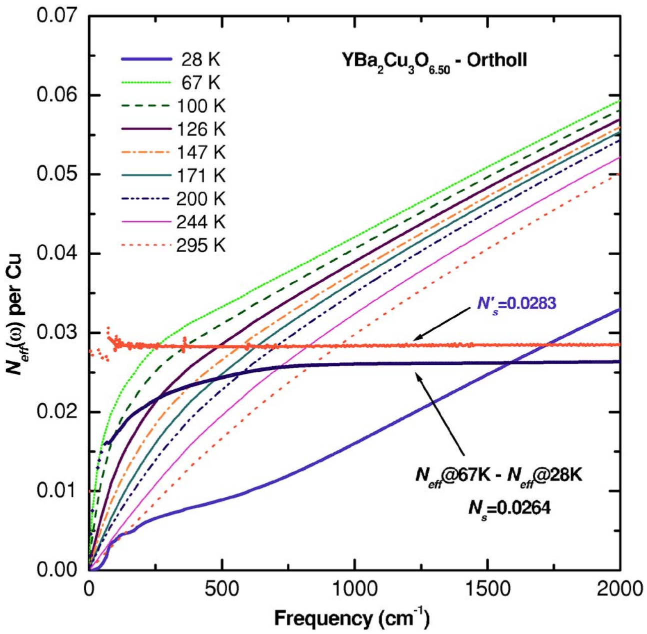

FIG. 4. (Color online) The partial spectral weight up to 2000 cm^{-1} shown as dashed and solid curves. The spectral weight increases monotonically with temperature and frequency except for the 28 K curve (heavy solid curve) in the superconducting state where there is a loss of spectral weight to the condensate and the curve is sharply lowered. The curve marked $N_s = N_{eff}(67\text{ K}) - N_{eff}(28\text{ K})$ is an estimate of the spectral weight of the superconducting condensate. The curve marked N_s' is a plot of the condensate density obtained independently from the imaginary part of $\sigma(\omega)$.

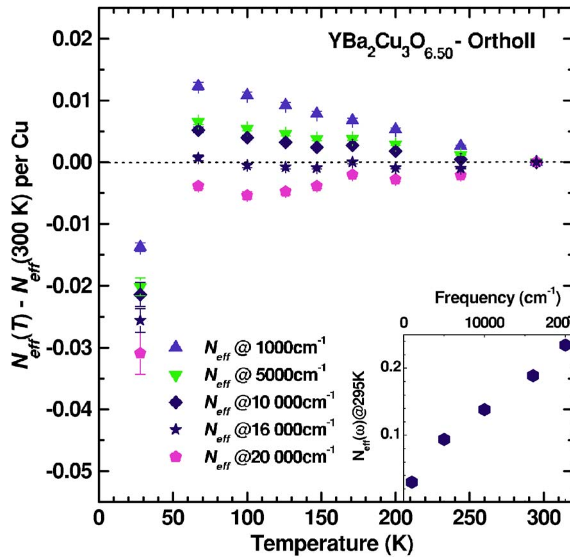

FIG. 5. (Color online) The partial spectral weight integrated up to various frequencies as a function of temperature. Below 16 000 cm^{-1} there is an increase in spectral weight as the temperature is lowered signaling a line narrowing on this frequency scale. Below T_c there is strong loss of spectral weight to the superconducting condensate. There is no evidence of any precursors to superconductivity at 67 K. In the inset we show $N_{eff}(\omega)$ at 295 K.

lowered. At lower frequencies, below 150 cm^{-1}, there appears to be an additional strong absorption band, but any structure here must be interpreted with caution since they are derived from reflectance data close to unity which are subject to large systematic errors. Finally, at higher frequencies, there is a broad continuous background absorption that extends up to the plasma frequency and has been attributed to the influence of strong correlations.[37,38]

We define the effective number of carriers per copper atom in terms of the partial sum rule: $N_{eff}(\omega) = (2meV_{Cu}/\pi e^2)\int_{0^+}^{\omega}\sigma_1(\omega')d\omega'$ where m is the free electron mass and V_{Cu} is the volume per copper atom, 57.7 Å^3. Figure 4 shows $N_{eff}(\omega)$ calculated from the optical conductivity. In the frequency region shown $N_{eff}(\omega)$ increase uniformly with frequency and temperature in the normal state.

In the superconducting state at 28 K, shown in Fig. 4 as a heavy solid curve, there is a dramatic loss of spectral weight due to the formation of the superconducting condensate. The effective number of carriers per copper atom in the condensate can be estimated from the partial sum rule by subtracting the normal state curve at 67 K from the superconducting curve at 28 K, also shown in the figure. The resulting difference curve rises rapidly at low frequency and saturates at a value of $N_s = 0.0264$ above 1000 cm^{-1}. To find a better value of N_s we need to estimate the normal state curve at 28 K. We do this by extrapolating the temperature dependence in the normal state to 28 K (see Fig. 5). With the corrected value of N_{eff} at 28 K we get a more accurate value of $N_s = 0.0276$. The condensate density can also be estimated from the imaginary part of the conductivity provided the contribution from the residual conductivity is not included, i.e., $N_s' = (mV_{Cu}/4e^2)\omega[\sigma_2(\omega) - \sigma_{2r}(\omega)] = 0.0283$ where σ_{2r} is the residual quasiparticle conductivity in the superconducting state. Figure 4 shows both N_s and N_s' and it is clear that the two curves (when corrected) approach one another closely and the two methods differ by 2.5% well within our 5% estimated experimental error. There have been several reports of *ab*-plane spectral weight changes on entering the superconducting state, in other high T_c cuprates[39–41] at the 1% to 2% level, but it should be noted that systematic errors in the absolute value of reflectance have a large influence on the magnitude of both N_s and N_s', although the error of the *difference* is smaller. We estimate that our error in N_s and N_s' is 30% but less than 5% in the difference $N_s' - N_s$. Thus, at this point, we are unable to conclude from our data that there is evidence for any added or missing low frequency spectral weight when the superconducting state forms in the Ortho-II Y123.

Figure 5 shows the temperature dependence of the partial spectral weight at various frequencies referred to the spectral weight at 300 K. We note that below 16 000 cm^{-1} the spectral weight increases as the temperature is lowered while above this frequency it is approximately temperature independent. Since this frequency is close to our estimate of the limit of the free carrier conductivity, we conclude that there is a transfer of spectral weight to low frequencies as the temperature is lowered within the free carrier band. We also note here that the temperature dependence of the partial spectral weight shows no sign of any precursors to superconductivity at 67 K which is 8 K above the bulk superconducting transition temperature.

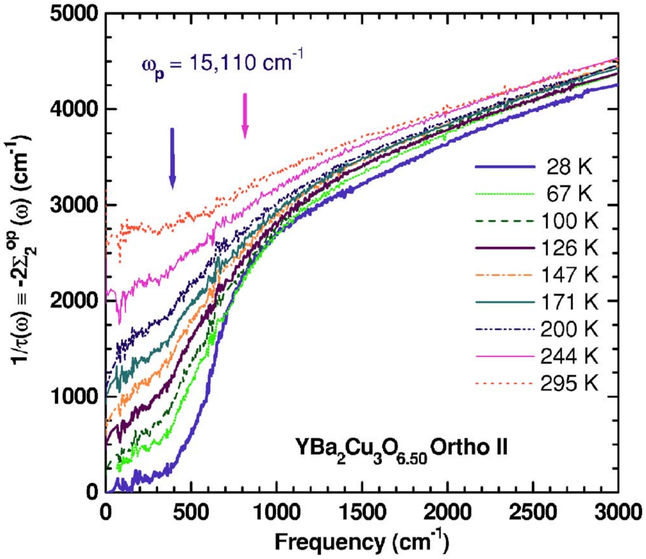

FIG. 6. (Color online) The optical scattering rate obtained from the extended Drude model. Two onsets, denoted by arrows dominate the scattering.

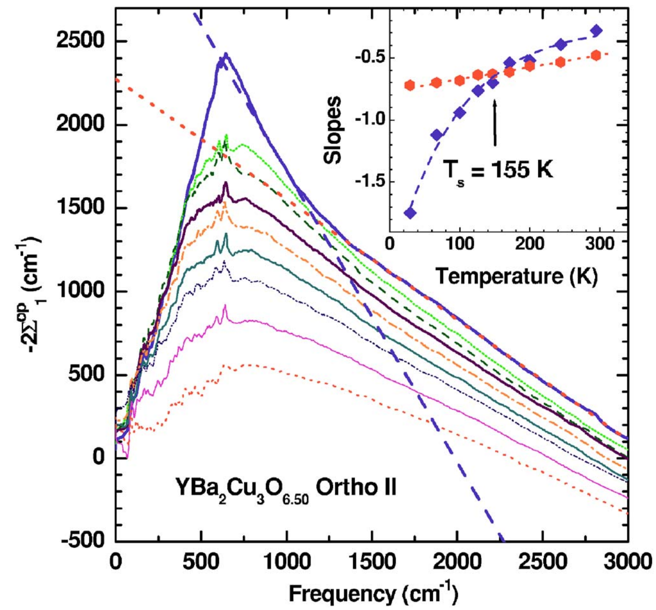

FIG. 7. (Color online) The optical self-energy. The imaginary part of the scattering rate is plotted. A broad peak is seen at 295 K (the lowest curve). As the temperature is lowered this peak splits into two components with a sharp peak appearing below 175 K as shown by the curvature change at this temperature. The inset shows a curvature analysis of the self-energy where the slope of the self-energy in the two regions, shown in the main panel as two dashed lines, have been plotted, circles, high frequency, and diamonds, low frequency.

The extended Drude model offers a detailed view of the charge carrier scattering spectrum and its contribution to the effective mass.[42] In this picture the scattering rate in the Drude expression is allowed to have a frequency dependence

$$\sigma(\omega,T) = i\frac{\omega_p^2}{4\pi}\frac{1}{\omega + [\omega\lambda(\omega,T) + i/\tau(\omega,T)]}$$
$$= i\frac{\omega_p^2}{4\pi}\frac{1}{\omega - 2\Sigma^{op}(\omega,T)}, \qquad (1)$$

where ω_p is the plasma frequency, $1/\tau(\omega,T)$ is the scattering rate and $\lambda(\omega)+1=m^*(\omega)/m$, $m^*(\omega)$ is an effective mass, and m the bare mass. We also introduce the optical self-energy $\Sigma^{op}\equiv\Sigma_1^{op}+i\Sigma_2^{op}$, where $-2\Sigma_1^{op}=\omega\lambda(\omega,T)$ and $-2\Sigma_2^{op}=1/\tau$. The optical self-energy is, apart from a $\cos(\theta)-1$ factor, where θ is a scattering angle, an average over the Fermi surface of the quasiparticle self-energy[16,17,43,44] as measured by the ARPES. Contrary to expectations, in optimally doped Bi-2212 where both optical and ARPES data exist, the self-energies derived from the two spectroscopies[45] are surprisingly similar to one another.[15,16,18]

Figure 6 shows the scattering rate calculated from the extended Drude model where $1/\tau(\omega,T)\equiv-2\Sigma_2^{op}(\omega,T)=(\omega_p^2/4\pi)\,\mathrm{Re}[1/\sigma(\omega,T)]$ for Ortho-II Y123. We also evaluate the real part of the optical self-energy, which is given by $-2\Sigma_1^{op}(\omega,T)=\omega\lambda(\omega,T)=-\omega_p^2/4\pi\,\mathrm{Im}[1/\sigma(\omega,T)]-\omega$ and is shown in Fig. 7. For the calculation of the optical self-energy and the scattering rate we need a value for the plasma frequency which includes spectral weight up to the interband transitions. Using a procedure adopted in a previous study[46] we find a plasma frequency ω_p=15 110 cm^{-1}.

In Fig. 6 we see an overall increase in scattering both with temperature and frequency. The frequency dependence is monotonic with two thresholds, shown with arrows, where the scattering rate undergoes a steplike increase, a prominent low frequency one at 400 cm^{-1} and a weaker, higher frequency one at 850 cm^{-1}. The variation of the scattering rate with temperature is roughly linear at low frequency, but becomes much weaker at high frequency above the high frequency threshold. The scattering rate is larger than the frequency at all temperatures except at 28 K in the superconducting state, i.e., $\hbar/\tau>\hbar\omega$.

In Fig. 7 we show the real part of the optical self-energy. It is related by Kramers-Kronig transformations to the scattering rate shown in Fig. 6. The separation of the two components of scattering is less obvious in this plot but in analogy with the Bi-2212 system where we have investigated the detailed doping dependent data on this quantity,[16] we find that the bosonic mode gives rise to a peak on top of a broader background. With increased underdoping in Bi-2212 the peak becomes triangular and harder to resolve from the background and is very similar in appearance to the Ortho-II Y123 data shown here. We can attempt to resolve the peak by focusing on the break in slope that occurs between 1000 cm^{-1} and 1400 cm^{-1} in the temperature range from 28 K to 171 K. Above 200 K the break in slope cannot be resolved, consistent with the notion that the curve has only one component. The inset to Fig. 7 shows a plot of the slopes of two straight dashed lines that have been fitted to the experimental data above and below the break frequency. We find that a plot of the two slopes crosses at 155 K, i.e., the second derivative of the optical self-energy goes through zero at this temperature and becomes uniformly positive, i.e., with only one component.

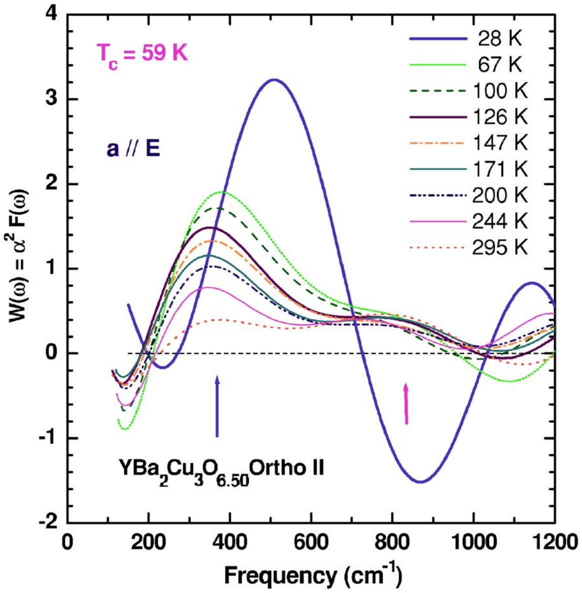

FIG. 8. (Color online) The Eliashberg function, $\alpha^2F(\omega)\approx W(\omega)$, which is calculated by using Eq. (2). We observe two peaks: one is temperature dependent at lower frequency and the other is temperature independent at higher frequency. In the superconducting state there is a large shift of the low energy peak and a dramatic overshoot of the scattering rate giving rise to a negative contribution to the Eliashberg function.

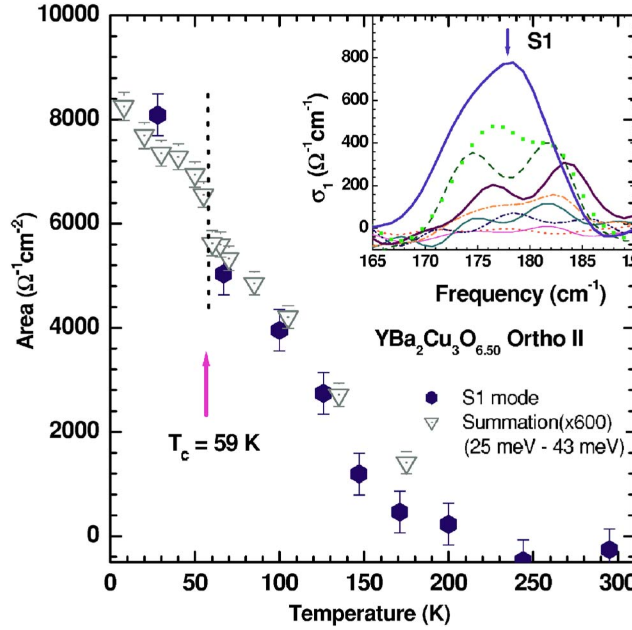

FIG. 9. (Color online) Area under the $S1$ mode as a function of temperature. We also show the area under the neutron resonance peak (Ref. 27) at $Q=(1/2,3/2,2.2)$ and 33.1 meV, solid triangles from 25 to 43 meV (open triangles) as a function of temperature. The inset shows the conductivity of the $S1$ mode with the background subtracted.

Recent calculations[21] of the self-energy of the charge carriers interacting with collective spin excitations suggest that the self-energy acquires an S-shaped frequency dependence in the presence of a sharp mode, whereas in the absence of such a mode the curve has a monotonically negative second derivative. From these observations we conclude, as a first approximation, that the bosonic mode is confined to temperatures below 155 K.

For another estimate of the strength of the interaction of the charge carriers with the sharp mode we used the procedure introduced by Marsiglio et al.[15,36,47] where the bosonic spectral function is derived from the second derivative of the optical scattering rate. This function can be written as follows:[36,42,48]

$$W(\omega)\equiv\frac{1}{2\pi}\frac{d^2}{d\omega^2}\left[\frac{\omega}{\tau(\omega)}\right] \qquad (2)$$

and $W(\omega)\approx\alpha^2F(\omega)$ at zero temperature in the normal state, where α is a coupling constant, and $F(\omega)$ is a bosonic density of states. The results are shown in Fig. 8. In this figure we show the function $W(\omega)$ calculated by fitting $1/\tau(\omega)$ from Fig. 6 to ten polynomial terms to obtain a smoothed second derivative.[48] The normal state shows two broad peaks; a prominent one at $\approx 350\ \mathrm{cm}^{-1}$ and a much weaker one at $\approx 800\ \mathrm{cm}^{-1}$. The higher frequency peak does not change with temperature while the lower frequency one grows monotonically as temperature decreases. Another interpretation is in terms of a temperature-dependent peak and a temperature-independent background, four times lower in amplitude. In the superconducting state there is a dramatic shift of the lower peak to higher frequency and the development of a region of negative spectral function $W(\omega)$ between 700 and $1000\ \mathrm{cm}^{-1}$. This behavior has been predicted by Abanov et al.[47]

Figure 9 shows the area under the peak $S1$ as a function of temperature obtained from a fit of a Lorentzian function to the conductivity peak. We see that the intensity of this feature decreases linearly with temperature going to zero at $\approx$200 K. On the same graph we have plotted the area under the neutron resonance and it is clear that the two phenomena have parallel temperature dependencies. We note that the spectral weight of the $S1$ peak, $3.1\times10^8\ \mathrm{cm}^{-2}$ represents only 0.16% of the total free carrier spectral weight, $1.94\times10^8\ \mathrm{cm}^{-2}$.

We note that to obtain a finite frequency absorption peak such as the peak $S1$, we need to break translational symmetry of the charge carriers. We can rule out phonon absorption which would be inconsistent with the large spectral weight of the peak $S1$ and the fact the spectral weight is temperature dependent as shown in Fig. 9. There are a number of possible candidate mechanisms but we would like to focus on the static charge-density patterns seen by scanning probe microscopy in Bi-2212.[49,50] Models for optical absorption by strip-like patterns have been described by Benfatto and Smith.[10] The model describes the optical absorption by charges confined by a static pinning potential with two parameters, the strength of the potential and the modulation amplitude.

Finally, we show the calculated dc resistivity extracted from the extrapolated zero frequency limit of the optical conductivity. Figure 10 shows the resulting dc resistivity for the eight normal state temperatures. The resistivity shows the

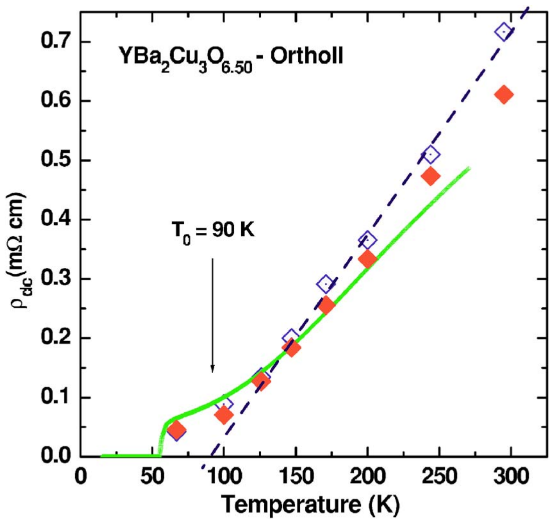

FIG. 10. (Color online) dc resistivity extracted from the optical conductivity by extrapolating the Kramers-Kronig derived optical conductivity to zero frequency (open diamonds) and from the Drude fit to reflectance (closed diamonds). The dashed line is a straight line fit to the open circles. The solid line is the dc resistivity measured by a four-probe resistance technique (Ref. 51). The temperature dependence shows the familiar linear variation with an intercept on the temperature axis of ≈90 K.

familiar linear temperature dependence with an intercept on the temperature axis of 90 K, typical of underdoped samples of high T_c cuprates. Also shown is the dc resistivity calculated from the fits to the reflectance with Drude peaks, shown in Fig. 2, as well the results for the four-probe dc resistance measurements on samples from the same source.[51] There is a 14% discrepancy in the slopes of the resistivity curves determined by the two optical techniques. We attribute this to different methods of determining the Drude plasma frequency. Where the two data sets are in good agreement is the value of ≈90 K for the intercept on the temperature axis. The dc resistivity points show a still lower value of the temperature resistivity slope.

II. DISCUSSION

We now turn to a general interpretation of our data in terms of models proposed for the electrodynamics of cuprates, focusing our attention on the low frequency spectral region below the free carrier plasma edge ≈10 000 cm^{-1}. It is clear from even the most superficial view of the data that the optical properties shown here are not those of a set of free carriers interacting weakly with impurities through elastic scattering or with lattice vibrations through inelastic scattering. Two approaches have been used to account for these deviations, the one and the two component models of conductivity. In the one component model any deviation from the simple Drude formula are attributed to a single set of charge carriers interacting with a variety of bosonic excitations while in the two component model a low frequency Drude component is separated by curve fitting and any remaining absorption is attributed to a mid-infrared band.

There is ample evidence that many conducting oxides do have a separate well-defined mid-infrared band with a peak frequency that moves to lower frequencies with doping.[52] This is also true of the one-layer cuprates, in particular $La_{2-x}Sr_xCuO_4$.[53] In some materials, when the peak reaches zero frequency, striking changes occur in the transport properties, for example, $Ba_{1-x}K_xBiO_3$ becomes superconducting at this doping level.[54] Recent evidence from thermal conductivity suggests that $La_{2-x}Sr_xCuO_4$ becomes an insulator below a doping level of 0.06 where superconductivity also sets in whereas Y123 remains in the conducting pseudogap state well below the doping level[55] of the superconductivity boundary. These observations suggest that the one-component to two-component transition occurs at different doping levels for these two materials and that the Y123 system remains metallic to the lowest doping levels. We conclude that, at least at the level of doping of ortho-II Y123, we are justified in using the one-component model.

The striking result of the one-component model is the strong frequency-dependent scattering rate $1/\tau(\omega,T)$ shown in Fig. 6. There is a nearly perfect linear variation of scattering at high frequency with a strong threshold at 400 cm^{-1} at low temperatures that gradually washes with increasing temperature. We will interpret our spectra within the one-component model in terms of a scattering rate that is averaged over the Brillouin zone and is the sum of two frequency-dependent terms, a bosonic mode that dominates at low temperature but whose spectral weight weakens as the temperature rises and a featureless temperature-independent background that extends to high frequencies.

Several theoretical models of strongly correlated system have been evoked to explain the strong linearly rising frequency dependent scattering rate. Earlier models included the marginal Fermi liquid,[56] the nested Fermi liquid models,[57] the nearly antiferromagentic liquid,[38,58] and the Luttinger liquid model.[37] All models predict a continuous linear rise of scattering governed by an energy scale of the order of ≈0.5 eV. The large energy scale rules out a simple phonon mechanism for the broad background scattering which would predict a flattening of the scattering rate beyond the maximum phonon frequency.[17] The strongly temperature-dependent threshold has generally been interpreted in terms of coupling to a bosonic mode,[13,14] in particular the the 41 meV magnetic resonance.[15–17]

A. Bosonic mode analysis of the optical scattering rate

Here we will adopt the approach of Schachinger *et al.*[17] and treat both the mode and the continuum scattering on an equal basis assuming that *both* originate from coupling of the charge carriers to bosonic fluctuations.

To study the temperature dependence of the coupling of bosonic modes to charge carriers we used the following expression to model the scattering rate within the extended Drude formalism:

$$\frac{1}{\tau(\omega,T)} = \frac{\pi}{\omega}\int_0^{+\infty} d\Omega\,\alpha^2F(\Omega)\int_{-\infty}^{+\infty} dz[N(z-\Omega)+N(-z+\Omega)] \times[n_B(\Omega)+1-f(z-\Omega)][f(z-\omega)-f(z+\omega)], \quad (3)$$

where $\alpha^2F(\Omega)$ is the bosonic spectral function,[59] $N(z)$ is the normalized density of state of the quasiparticles, $n_B(\Omega) = 1/(e^{\beta\Omega}-1)$, $f(z)=1/(e^{\beta z}+1)$ are the boson and fermion occupation numbers, respectively, and $\beta=1/(k_BT)$.

Equation (3) represents a finite temperature generalization of the $T=0$ expression[60]

$$\frac{1}{\tau(\omega)} = \frac{2\pi}{\omega}\int_0^{\omega} d\Omega \alpha^2 F(\Omega) \int_0^{\omega-\Omega} dz \frac{1}{2}[N(z)+N(-z)]. \quad (4)$$

Equation (3) is derived using the method proposed by Shulga *et al.*[61] and its derivation will be given elsewhere.[62] Both Eqs. (3) and (4) are suitable for the case when the quasiparticle density of states, $N(z)$, cannot be taken as constant in the vicinity of the Fermi levels, e.g., in the pseudogap state.

The density of state $N(z)$ was modeled with a pseudogap with a quadratic gap function

$$N(z) = \left[N(0) + [1-N(0)]\frac{z^2}{\Delta^2}\right]\theta(\Delta - |z|) + \theta(|z| - \Delta), \quad (5)$$

where $1-N(0)$ is the depth of the gap, $\theta(z)$ is the Heaviside step function, and $\Delta=350$ cm^{-1} is the frequency width of the gap based on spectroscopic data for the pseudogap from tunneling[63] and c-axis infrared conductivity.[64] An example for a depth of the gap of 0.50 is shown in Fig. 13.

For the bosonic spectral function $\alpha^2F(\Omega)$ we used the sum of two functions, a peak and a background,

$$\alpha^2 F(\Omega) = PK(\Omega) + BG(\Omega). \quad (6)$$

$$PK(\Omega) = \frac{A}{\sqrt{2\pi}(d/2.35)} e^{-(\Omega - \Omega_{PK})^2/[2(d/2.35)^2]}, \quad (7)$$

$$BG(\Omega) = \frac{I_s \Omega}{\Omega_0^2 + \Omega^2}, \quad (8)$$

where $PK(\Omega)$ is a Gaussian peak and $BG(\Omega)$ is the background which we have modeled on the spin fluctuation spectrum of Millis, Monien, and Pines (MMP).[38] A is the area under the Gaussian peak, d is the full width at half maximum (FWHM), and Ω_{PK} is its center frequency. We fixed the parameters of the Gaussian peak to values shown in Table II based on the inelastic neutron scattering results of Stock *et al.*[65] I_s is the intensity of the MMP background and Ω_0 is the frequency of the background at maximum. The complete bosonic spectral function $\alpha^2F(\Omega)$ used is shown in Fig. 11. It has two adjustable parameters, the amplitude of the Gaussian peak A and depth of the pseudogap $1-N(0)$. All the other parameters have been determined from other experiments.

We used least squares to fit our scattering rate data shown in Fig. 6 to Eq. (3). The amplitude of the MMP background and its center frequency were determined by fitting the data at 295 K including only the MMP background in $\alpha^2F(\Omega)$ with a very shallow gap (see Table II) in the fermion density of states $N(z)$. We fixed the background parameters for all other lower temperatures to their 295 K values. For further fits at lower temperatures, only two free parameters were used: the depth of the gap in the density of states and the area under the resonance peak, A. The calculated $1/\tau(\omega)$ spectra are compared with the measured data in Fig. 12. The dimensionless coupling constant or mass enhancement factor λ is defined as

TABLE II. The parameters of the bosonic mode analysis at six representative temperatures, $T=67$, 100, 147, 200, 244, and 295 K. The peak is a Gaussian function [see Eq. (8)] and MMP is the background [see Eq. (9)]. The quantities λ_{PK} and λ_{BG} are the coupling constants for the peak and the MMP background, respectively. The depth, $1\times N(0)$, is the depth of the gap at Fermi level in the density of state. All the frequencies are measured in cm^{-1}.

Temperature (K)	Peak A	Peak Ω_{PK}	Peak d	Peak λ_{PK}	MMP I_s	MMP Ω_0	MMP λ_{BG}	Depth $1\times N(0)$
67	255	248	80	2.20	354	320	3.30	0.413
100	235	248	80	1.93	354	320	3.30	0.413
147	170	248	80	1.40	354	320	3.30	0.386
200	105	248	80	0.86	354	320	3.30	0.411
244	62	248	80	0.51	354	320	3.30	0.366
295	0	248	80	0.00	354	320	3.30	0.172

$$\lambda = 2\int_0^{\infty} d\Omega \frac{\alpha^2 F(\Omega)}{\Omega}. \quad (9)$$

The contributions to λ_{PK} and λ_{BG}, from the peak and the background as well as other parameters of the model are shown in Table II.

One result of our fit is the temperature dependence of the depth of the pseudogap shown in the lower panel of Fig. 13. The depth, we find, corresponds to a 41% depression of the

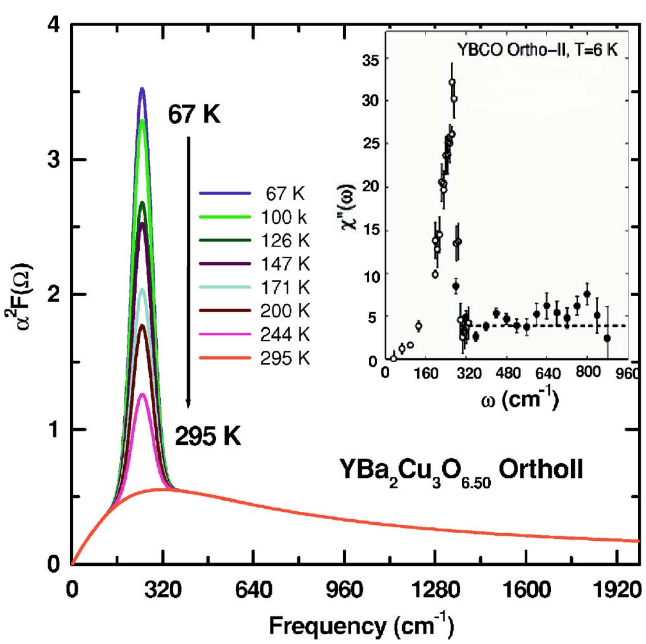

FIG. 11. (Color online) The bosonic spectral function $\alpha^2F(\Omega)$ obtained from the least square fits to the experimental data. In the inset we show $\chi''(\omega)$ determined by neutron scattering from Fig. 13 in Ref. 65.

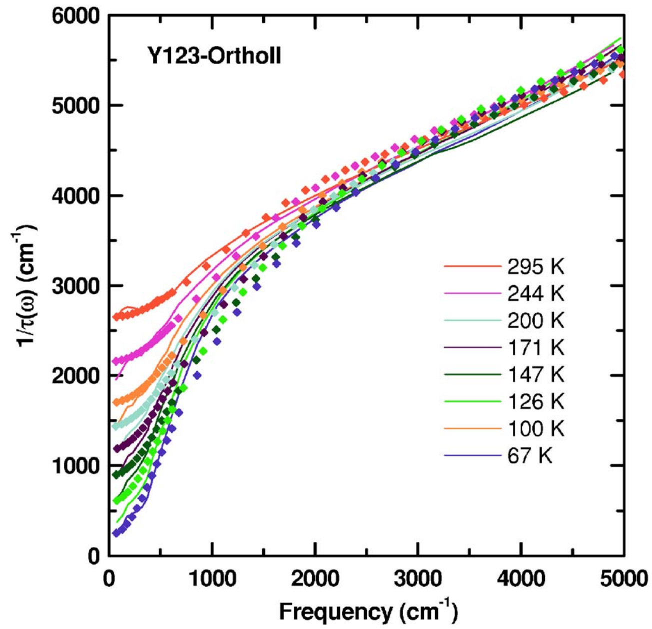

FIG. 12. (Color online) The optical scattering rates (solid lines) and our fits (symbols) based on Eq. (3) with the bosonic spectral function shown in Fig. 11 and pseudogap information of Fig. 13 for the normal states. We note that the negative temperature dependence of the mode contribution combined with the almost equal and opposite contribution of the background results in a nearly temperature independent scattering rate at high frequencies, in complete agreement with the experimental results.

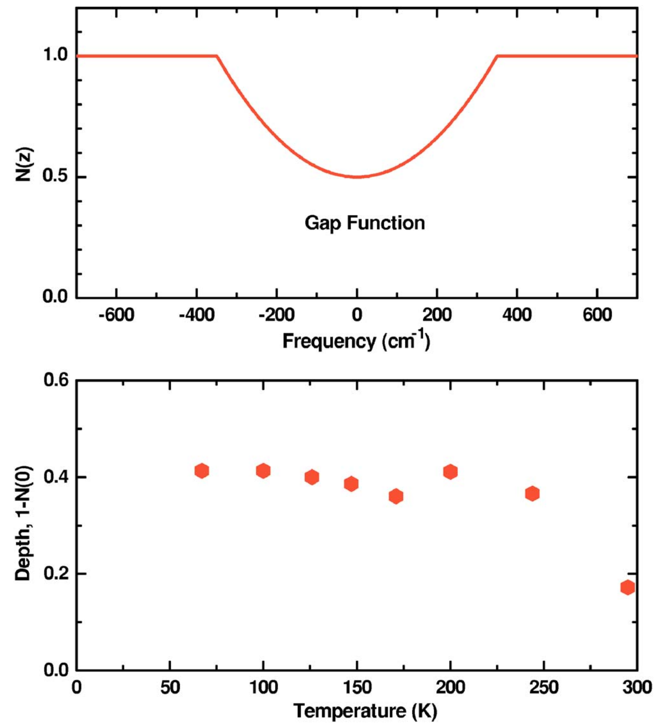

FIG. 13. (Color online) The upper panel shows the quasiparticle density of state with a gap, $N(z)$. The lower panel shows the depth of the pseudogap for the least square fits. The other parameters of the fit are shown in Table II.

density of states at low temperature decreasing gradually to 17% at room temperature. The depth of the pseudogap in the c-axis optical conductivity is more pronounced[64] but it is known that c-axis transport is weighted more heavily in the antinodal direction where the pseudogap is deeper whereas ab-plane transport is more evenly distributed in momentum space.

Next, we compare our spectral function $\alpha^2F(\Omega)$ in Fig. 11 with the magnetic susceptibility $\chi''(\omega)$ determined by neutron scattering at 6 K ($<T_c$) by Stock *et al.* (see the inset in Fig. 11). The two sets of curves are very similar although it should be pointed out that our data are in the normal states and neutron data are in the superconducting state and that the *width* of our mode has been set equal to that of the neutron resonance mode.

Comparing the relative amplitudes of the peak and the background, we find a substantial difference with the neutron data. For the ratio of the background to the peak amplitude our $\alpha^2F(\Omega)$ at 67 K gives $\sim$0.17 while the neutron $\chi''(\omega)$ gives $\sim$0.27 in the normal state (we estimated the ratio in the normal state from the temperature dependent intensity of the neutron mode[27]). The relative amplitude of the peak in our spectra is 63% stronger than what is seen by neutron scattering. In the absence of a more detailed calculation of the spectral function, this discrepancy is not surprising since the coupling of the charge carriers to spin fluctuations involves integrations over the Fermi surface and we are reporting only on weighted averages. On the other hand, our data leaves open the possibility that the high frequency channel of conductivity, which is active in producing our background, is not well described by the MMP spin fluctuations. In addition to the relative amplitudes we can also compare the areas under the peak and background spectral functions. There is a sum rule for the area under $\chi''(\omega)$ which is related to our optical function $\alpha^2F(\Omega)$ by a coupling constant, g^2. Neutron scattering finds that the area under the spin resonance is about 3% of the total area. In our case at 67 K this fraction is about 25%, considerably larger. It can be argued that the coupling to the resonance $\underline{g^2}$ could be larger than its background value by a factor of $\sim\sqrt{8}$. This is reasonable since the resonance is around (π,π), where the susceptibility is also expected to peak.

In Fig. 14 we compare three quantities: the total area under the magnetic susceptibility in the 25 to 43 meV energy range from Stock *et al.*,[27] the area under the peak at 350 cm^{-1} in the $W(\Omega)\approx\alpha^2F(\Omega)$ obtained from the second derivative of $1/\tau(\omega)$, and the area under the peak at 248 cm^{-1} in the $\alpha^2F(\Omega)$ from our fit. We note that the two areas from the two different procedures for deriving $\alpha^2F(\Omega)$ show almost identical temperature dependencies. The area under the peak obtained from the magnetic susceptibility shows a temperature trend similar to those of the optical data.

III. DISCUSSION AND CONCLUSIONS

A. The two channels of scattering of the charge carriers

In analyzing the optical properties of Ortho-II Y123 we have adopted the one-component model of conductivity, at-

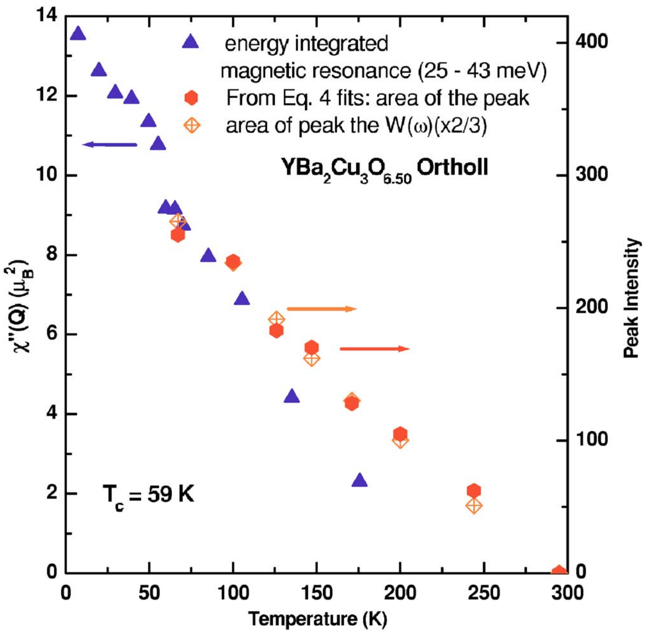

FIG. 14. (Color online) Temperature dependence of the amplitude of the sharp mode. The open diamonds with cross are from the second derivative analysis of the scattering rate; the closed hexagons are from fit a scattering rate to the model, including a sharp mode and a background. The upright triangles show the energy integrated amplitude of the neutron mode Stock *et al.* (Ref. 27).

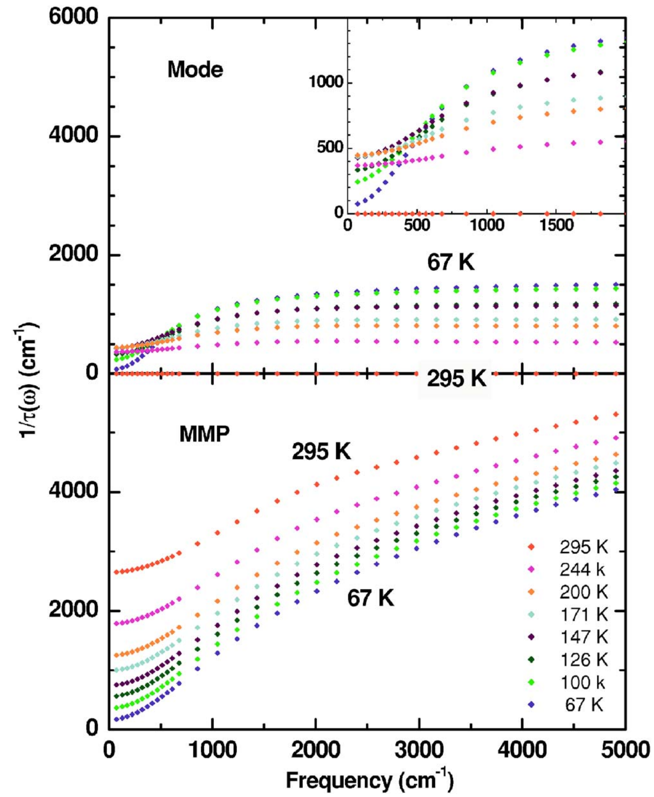

FIG. 15. (Color online) The mode contribution (upper panel) and the MMP back ground contribution (lower panel) on the scattering rate based on Eq. (3) with the parameter shown in Table II and pseudogap information of Fig. 13 for the normal states. We note at high frequencies the opposite temperature dependencies of the mode and the background contributions.

tributing any deviations from the simple Drude formula to inelastic processes. We find that the high frequency processes are well described by the MMP spectrum of spin fluctuations with a temperature dependence that originates in the bosonic occupation numbers, but a temperature-*independent* spectral function, while at lower frequencies a strong temperature dependence sets in and the conductivity is well described by the extended Drude model with a temperature-*dependent* spectral function.

The two methods we used to estimate the shape and temperature dependence of the bosonic spectrum gave very similar results. The main contribution to the spectral weight came from a prominent peak at 350 cm^{-1} which was strongly temperature dependent in strength. From this temperature dependence we identified the mode with the neutron resonance which has a frequency of 248 cm^{-1}. The 100 cm^{-1} discrepancy we attributed to the effect of the pseudogap in the density of states which, as calculations suggest, has the effect of shifting upward the frequency of any bosonic mode. To fit the data, the strength of the mode had to be temperature dependent and the electronic density of states had to have a gap whose depth was also temperature dependent. These observations are in accord with what is known about the normal state of underdoped Y123 from other experiments.

The properties of the sharp bosonic resonance in the infrared scattering rate agree with the properties of the (π,π) spin-flip neutron resonance mode. The frequency of the bosonic resonance 248 cm^{-1} or 31 meV agrees with the frequency of the neutron mode measured by Stock *et al.*[27] (provided the pseudogap is included in the model). The temperature dependence of the strength of the mode also agrees with the neutron measurements on Ortho-II Y123 samples from the same source. The total spectral weight of the mode determined from least squares fits drops monotonically with temperature and reaches zero between 200 and 300 K, in agreement with the spectral weight of the neutron mode.

Figure 15 shows separately the two contributions to the scattering rate. We see that the combination of a sharp mode whose strength decreases with temperature and a temperature independent background suggests a solution to a long-standing problem in the optical conductivity of the cuprates: there is a strong temperature dependence at low frequencies but above 500 cm^{-1} the scattering is nearly temperature independent. In the picture of mode and background, both caused by coupling to bosons, this high frequency behavior is the result of a competition between a rising absorption due to occupancy of the background boson population and a decrease in the strength of the bosonic mode with temperature. This scenario predicts an overall linear temperature dependence at all frequencies above the temperature where the sharp mode disappears. There is some evidence for this kind of behavior in the data for $La_{2-x}Sr_xCuO_4$ which does not have a magnetic resonance but shows a linear temperature dependence characteristic of bosons both in the dc resistivity[66] and optical scattering rate at high frequency.[67]

Finally we note that in an early paper by Collins *et al.*[68] on the *ab* plane reflectance of $YBa_2Cu_3O_{6+x}$, a fit similar to ours has been performed, but without any prejudgment about the shape of the bosonic spectral function, since at the time, neither the magnetic resonance nor the MMP background functions had been discovered. The authors found an $\alpha^2F(\Omega)$ curve very similar to our Fig. 11 with a peak at 250 cm^{-1} and a background extending to 2500 cm^{-1} (although the authors say that the background above 800 cm^{-1} should be ignored). The authors also note that their model predicts a larger temperature dependence than what they observe. This is consistent with our conclusions that the sharp bosonic mode intensity has a strong temperature dependence.

B. Summary and conclusion

In summary, we have shown that two optical phenomena in Ortho-II Y123 have a close association with the magnetic resonance as measured for samples from the same source. The first is the onset of scattering associated with a bosonic resonance. This has been suggested by several previous investigators,[15–17,20] but here, we base our conclusions on experiments that use crystals with the same, well-defined doping level grown by the same technique.

The second is the low-temperature conductivity peak that we have designated $S1$. Its connection to the magnetic resonance is not obvious since the magnetic resonance by itself is not optically active. The peak $S1$ may be a plasma resonance associated with in-plane charge density modulations either through pinning to defects[10] or through a transverse plasma resonance associated with the inhomogeneous charge density that seems to be present in underdoped cuprates in the normal state.[49,50] We still need to connect such a charge ordered state to the magnetic resonance. One possible mechanism is the growth of in-plane coherence that takes place in the temperature region just above T_c. An example of this kind of behavior is the transverse plasma resonance that is seen in interplane conductivity. It is based on the charge inhomogeneity associated with the double layer structure but becomes optically active only at low temperature, tracking the temperature dependence of the magnetic resonance.[69]

ACKNOWLEDGMENTS

This work has been supported by the Canadian Natural Science and Engineering Research Council and the Canadian Institute of Advanced Research. We would like to thank Artem Abanov, Elena Banscones, Dimitri Basov, Lara Benfatto, Andrey Chubukov, Chris Homes, Peter Johnson, Alexandra Lanzara, Boza Mitrovic, Mike Norman, Brian Statt (deceased), Setsuko Tajima, David Tanner, Tony Valla, and Zahra Yamani for helpful discussions.

*Electronic address: timusk@mcmaster.ca

[1] For a review see: T. Timusk and B. Statt, Rep. Prog. Phys. **62**, 61 (1999); an update to this review can be found in T. Timusk, Solid State Commun. **127**, 337 (2003).
[2] J. Rossat-Mignod, L. P. Regnault, C. Vettier, P. Bourges, P. Burlet, J. Bossy, J. Y. Henry, and G. Lapertot, Physica C **185-189**, 86 (1991).
[3] H. A. Mook, Pengcheng Dai, S. M. Hayden, G. Aeppli, T. G. Perring, and F. Do, Nature (London) **395**, 580 (1998).
[4] H. F. Fong, P. Bourges, Y. Sidis, L. P. Regnault, A. Ivanov, G. D. Gu, N. Koshizuka, and B. Keimer, Nature (London) **398**, 588 (1999).
[5] Z. A. Xu, N. P. Ong, Y. Wang, T. Kakeshita, and S. Uchida, Nature (London) **406**, 486 (2000).
[6] N. P. Ong, Y. Wang, S. Ono, Y. Ando, and S. Uchida, Ann. Phys. **13**, 9 (2004).
[7] J. M. Tranquada, B. J. Sternlieb, J. D. Axe, Y. Nakamura, and S. Uchida, Nature (London) **375**, 561 (1995).
[8] M. Dumm, D. N. Basov, S. Komiya, Y. Abe, and Y. Ando, Phys. Rev. Lett. **88**, 147003 (2002).
[9] A. Lucarelli, S. Lupi, M. Ortolani, P. Calvani, P. Maselli, M. Capizzi, P. Giura, H. Eisaki, N. Kikugawa, T. Fujita, M. Fujita, and K. Yamada, Phys. Rev. Lett. **90**, 037002 (2003).
[10] L. Benfatto and C. M. Smith, Phys. Rev. B **68**, 184513 (2003).
[11] V. J. Emery and S. A. Kivelson, Nature (London) **374**, 434 (1995).
[12] J. Corson, R. Malozzi, J, Orenstein, J. N. Eckstein, and I. Bozovic, Nature (London) **398**, 221 (1999)..
[13] G. A. Thomas, J. Orenstein, D. H. Rapkine, M. Capizzi, A. J. Millis, R. N. Bhatt, L. F. Schneemeyer, and J. V. Waszczak, Phys. Rev. Lett. **61**, 1313 (1988).
[14] A. V. Puchkov, D. N. Basov, and T. Timusk, J. Phys.: Condens. Matter **8**, 10049 (1996).
[15] J. P. Carbotte, E. Schachinger, and D. N. Basov, Nature (London) **401**, 354 (1999).
[16] J. Hwang, T. Timusk, and G. D. Gu, Nature (London) **427**, 714 (2004).
[17] E. Schachinger, J. J. Tu, and J. P. Carbotte, Phys. Rev. B **67**, 214508 (2003).
[18] M. R. Norman and H. Ding, Phys. Rev. B **57**, R11089 (1998).
[19] M. Eschrig and M. R. Norman, Phys. Rev. B **67**, 144503 (2003).
[20] P. D. Johnson, T. Valla, A. V. Fedorov, Z. Yusof, B. O. Wells, Q. Li, A. R. Moodenbaugh, G. D. Gu, N. Koshizuka, C. Kendziora, S. Jian, and D. G. Hinks, Phys. Rev. Lett. **87**, 177007 (2001).
[21] A. V. Chubukov and M. R. Norman, Phys. Rev. B **70**, 174505 (2004).
[22] J. F. Zasadzinski, L. Ozyuzer, N. Miyakawa, K. E. Gray, D. G. Hinks, and C. Kendziora, Phys. Rev. Lett. **87**, 067005 (2001).
[23] A. Lanzara, P. V. Bogdanov, X. J. Zhou, S. A. Kellar, D. L. Feng, E. D. Lu, T. Yoshida, H. Eisaki, A. Fujimori, K. Kishio, J.-I. Shimoyama, T. Noda, S. Uchida, Z. Hussain, and Z.-X. Shen, Nature (London) **412**, 510 (2001).
[24] H. Y. Kee, S. A. Kivelson, and G. Aeppli, Phys. Rev. Lett. **88**, 257002 (2002).
[25] Ruixing Liang, D. A. Bonn, and Walter N. Hardy, Physica C **336**, 57 (2000).
[26] Z. Yamani, W. A. MacFarlane, B. W. Statt, D. Bonn, R. Liang, and W. N. Hardy, Physica C **405**, 227 (2004).
[27] C. Stock, W. J. L. Buyers, R. Liang, D. Peets, Z. Tun, D. Bonn, W. N. Hardy, and R. J. Birgeneau, Phys. Rev. B **69**, 014502

(2004).
[28] Ruixing Liang, D. A. Bonn, and W. N. Hardy, Physica C **304**, 105 (1998).
[29] C. C. Homes, M. A. Reedyk, D. A. Crandles, and T. Timusk, Appl. Opt. **32**, 2976 (1993).
[30] M. K. Crawford, G. Burns, and F. Holtzberg, Solid State Commun. **70**, 557 (1989).
[31] S. Tajima, T. Ido, S. Ishibashi, T. Itoh, H. Eisaki, Y. Mizuo, T. Arima, H. Takagi, and S. Uchida, Phys. Rev. B **43**, 10496 (1991).
[32] C. C. Homes, A. W. McConnell, B. P. Clayman, D. A. Bonn, Ruixing Liang, W. N. Hardy, M. Inoue, H. Negishi, P. Fournier, and R. L. Greene, Phys. Rev. Lett. **84**, 5391 (2000).
[33] T. Pereg-Barnea, P. J. Turner, R. Harris, G. K. Mullins, J. S. Bobowski, M. Raudsepp, Ruixing Liang, D. A. Bonn, and W. N. Hardy, Phys. Rev. B **69**, 184513 (2004).
[34] Frederick Wooten, *Optical Properties of Solids* (Academic, New York, 1972).
[35] H. Romberg, N. Nücker, J. Fink, Th. Wolf, X. X. Xi, B. Koch, H. P. Geserich, M. Dürrler, W. Assmus, and B. Gegenheimer, Z. Phys. B: Condens. Matter **78**, 367 (1990).
[36] F. Marsiglio, T. Startseva, and J. P. Carbotte, Phys. Lett. A **245**, 172 (1998).
[37] P. W. Anderson, Phys. Rev. B **55**, 11785 (1997).
[38] A. J. Millis, H. Monien, and D. Pines, Phys. Rev. B **42**, 167 (1990).
[39] D. B. Tanner, Y.-D. Yoon, A. Zibold, H. L. Liu, M. A. Quijada, S. W. Moore, J. M. Graybeal, B.-H. O, J. T. Markert, R. J. Kelley, M. Onellion, and J.-H. Cho, in *Spectroscopic Studies of Superconductors*, edited by Ivan Bozovic and Dirk van der Marel [Proc. SPIE **13**, 2696 (1996)].
[40] A. F. Santander-Syro, R. P. S. M. Lobo, N. Bontemps, Z. Konstantinovic, Z. Z. Li, and H. Raffy, Europhys. Lett. **62**, 568 (2003).
[41] H. J. A. Molegraaf, C. Presura, D. van der Marel, P. H. Kes, and M. Li, Science **295**, 2239 (2002).
[42] P. B. Allen, Phys. Rev. B **3**, 305 (1971).
[43] A. Kaminski, J. Mesot, H. Fretwell, J. C. Campuzano, M. R. Norman, M. Randeria, H. Ding, T. Sato, T. Takahashi, T. Mochiku, K. Kadowaki, and H. Hoechst, Phys. Rev. Lett. **84**, 1788 (2000).
[44] A. J. Millis and H. D. Drew, Phys. Rev. B **67**, 214517 (2003).
[45] J. P. Carbotte, E. Schachinger, and J. Hwang, Phys. Rev. B **71**, 054506 (2005).
[46] J. Hwang, T. Timusk, A. V. Puchkov, N. L. Wang, G. D. Gu, C. C. Homes, J. J. Tu, and H. Eisaki, Phys. Rev. B **69**, 094520 (2004).
[47] A. Abanov, A. V. Chubukov, and J. Schmalian, Phys. Rev. B **63**, 180510(R) (2001).
[48] J. J. Tu, C. C. Homes, G. D. Gu, D. N. Basov, and M. Strongin, Phys. Rev. B **66**, 144514 (2002).
[49] M. Vershinin, S. Misra, S. Ono, Y. Abe, Y. Ando, and A. Yazdani, Science **303**, 1995 (2004).
[50] K. McElroy, D.-H. Lee, J. E. Hoffman, K. M. Lang, J. Lee, E. W. Hudson, H. Eisaki, S. Uchida, and J. C. Davis, Phys. Rev. Lett. **94**, 197005 (2005).
[51] M. L. Sutherland, thesis, University of Toronto, 2004.
[52] S. Uchida, T. Ido, H. Takagi, T. Arima, Y. Tokura, and S. Tajima, Phys. Rev. B **43**, 7942 (1991).
[53] S. L. Herr, K. Kamaras, C. D. Porter, M. G. Doss, D. B. Tanner, D. A. Bonn, J. E. Greedan, C. V. Stager, and T. Timusk, Phys. Rev. B **36**, 733 (1987).
[54] A. V. Puchkov, T. Timusk, M. A. Karlow, S. L. Cooper, P. D. Han, and D. A. Payne, Phys. Rev. B **54**, 6686 (1996).
[55] M. Sutherland, S. Y. Li, D. G. Hawthorn, R. W. Hill, F. Ronning, M. A. Tanatar, J. Paglione, H. Zhang, L. Taillefer, J. DeBenedictis, Ruixing Liang, D. A. Bonn, and W. N. Hardy, Phys. Rev. Lett. **94**, 147004 (2005).
[56] P. B. Littlewood and C. M. Varma, J. Appl. Phys. **69**, 4979 (1991).
[57] P. Prelovsek, T. Tohyama, and S. Maekawa, Phys. Rev. B **64**, 052512 (2001).
[58] P. Monthoux and D. Pines, Phys. Rev. B **47**, 6069 (1993).
[59] J. P. Carbotte, Rev. Mod. Phys. **62**, 1027 (1990).
[60] B. Mitrovic and M. A. Fiorucci, Phys. Rev. B **31**, 2694 (1985).
[61] S. V. Shulga, O. V. Dolgov, and E. G. Maksimov, Physica C **178**, 266 (1991).
[62] S. G. Sharapov and J. P. Carbotte, Phys. Rev. B **72**, 134506 (2005).
[63] M. Kugler, Ø. Fischer, Ch. Renner, S. Ono, and Yoichi Ando, Phys. Rev. Lett. **86**, 4911 (2001).
[64] C. C. Homes, T. Timusk, R. Liang, D. A. Bonn, and W. N. Hardy, Phys. Rev. Lett. **71**, 1645 (1993).
[65] C. Stock, W. J. L. Buyers, R. A. Cowley, P. S. Clegg, R. Coldea, C. D. Frost, R. Liang, D. Peets, D. Bonn, W. N. Hardy, and R. J. Birgeneau, Phys. Rev. B **71**, 024522 (2005).
[66] M. Gurvitch and A. T. Fiory, Phys. Rev. Lett. **59**, 1337 (1987).
[67] T. Startseva, T. Timusk, A. V. Puchkov, D. N. Basov, H. A. Mook, M. Okuya, T. Kimura, and K. Kishio, Phys. Rev. B **59**, 7184 (1999).
[68] R. T. Collins, Z. Schlesinger, F. Holtzberg, P. Chaudhari, and C. Feild, Phys. Rev. B **39**, 6571 (1989).
[69] T. Timusk and C. C. Homes, Solid State Commun. **126**, 63 (2003).